frontiers | Frontiers in Materials

TYPE Original Research
PUBLISHED 09 August 2024
DOI 10.3389/fmats.2024.1431648

OPEN ACCESS

EDITED BY
Ferhun Caner,
Universitat Politecnica de Catalunya, Spain

REVIEWED BY
Grzegorz Golewski,
Lublin University of Technology, Poland
Babür Deliktas,
Bursa Uludağ University, Türkiye
Weipei Xue,
Anhui University of Science and Technology, China

*CORRESPONDENCE
Li Chen,
1063915947@qq.com

RECEIVED 12 May 2024
ACCEPTED 23 July 2024
PUBLISHED 09 August 2024

CITATION
Zhao Q, Chen L, Wang X, Zhang S and Li F (2024) Study on the modification effect and mechanism of composite solid waste and steel fiber on the mechanical properties of concrete.
Front. Mater. 11:1431648.
doi: 10.3389/fmats.2024.1431648

Study on the modification effect and mechanism of composite solid waste and steel fiber on the mechanical properties of concrete

Qingming Zhao[1], Li Chen[1]*, Xiaoyu Wang[2], Shengru Zhang[1] and Fan Li[3]

[1]School of Civil Engineering, Changchun Institute of Technology, Changchun, China, [2]Shanxi Architectural Design and Research Institute Co., Ltd., Taiyuan, China, [3]School of Traffic Engineering, Wuhan Vocational College of Transportation, Wuhan, China

To promote the use of solid waste in concrete production and solve the problem of secondary pollution caused by a large amount of solid waste, the four-factor and four-level orthogonal test method was used to investigate the different replacement rates of coal gangue (CG) ceramics (15%, 20%, 25%, and 30%), coal gangue ceramic sand (CGS) (10%, 15%, 20%, and 25%), fly ash (FA) (10%, 15%, 20%, and 25%), and steel fiber (SF) content (0.30%, 0.60%, 0.90%, and 1.2). By using range analysis, variance analysis, matrix analysis, and regression analysis, the prediction models of primary and secondary factors, optimal dosage, and strength under different factor levels were obtained. The microstructure and strengthening mechanisms of different materials were analyzed by scanning electron microscopy (SEM). The results show that the optimal combination of the CG substitution rate is 30%, CGS substitution rate is 15%, SF content is 1.2%, and FA substitution rate is 10% for cube compressive strength. For the splitting tensile strength, the optimal combination is a CG substitution rate of 30%, CGS substitution rate of 25%, SF content of 1.2%, and FA substitution rate of 10%. The resulting strength prediction model has high accuracy, which can predict the strength within the range selected by the orthogonal test in this paper and provide a reference for the application of steel fibers and solid waste in concrete, which contributes to the energy conservation and emission reduction in the construction industry.

KEYWORDS

solid waste, coal gangue, steel fiber, fly ash, mechanical strength

1 Introduction

Continuously accelerating urbanization, rapid economic growth, and other issues have greatly accelerated solid waste generation, which has become a global environmental problem (Song et al., 2015; Nayanathara Thathsarani Pilapitiya and Ratnayake, 2024). The construction industry is a field that consumes a large amount of solid waste due to its large capacity (Patel et al., 2023; Roy and Islam, 2024). The use of solid waste in concrete instead

of cementitious materials or natural aggregates can not only reduce the mining of natural aggregates and save resources but also delay the secondary environmental pollution caused by massive accumulation (Yu et al., 2022; Zhu et al., 2022).

A large number of experts and scholars have carried out much research on the application of solid waste in the construction industry. Wang et al. (2024) investigated slag, fly ash (FA), and other materials involved in preparing solid waste-based binders and studied their mechanical properties and shrinkage characteristics. Moussadik et al. (2024) studied the mechanical properties of light-weight aerated concrete mixed with coal gangue (CG) and fly ash and used XRD, SEM-EDS, and other technologies to study the microstructure characteristics, providing a new idea for solid waste recycling. Guo et al. (2022) used coal gangue, fly ash, and slag to prepare low-cost geopolymer grouting materials; analyzed the fluidity, permeation resistance, and mechanical properties of the geopolymer under different dosages by using the response surface method; and obtained the optimal mixing ratio of fly ash: slag: coal gangue: 1:4:5. Li et al. (2023a) used the microbial method to prepare coal gangue and fly ash into backfill materials and studied the influence of bacterial concentration, curing time, curing temperature, and other factors on the compressive strength, providing a theoretical basis for solid waste in coal mine backfill gob. Li et al. (2024) designed five kinds of substitution rates with 20% intervals, used coal gangue as a coarse aggregate to prepare concrete-filled steel tube columns, and studied the effect of coal gangue and fly ash in concrete-filled steel tube columns. Golewski (2022); Golewski (2023a); Golewski (2023b); Golewski (2023c); Golewski (2023d); Golewski (2024) team studied the strength, fracture toughness, water absorption, and microstructure of concrete composite materials after addition of fly ash and nano-silica. Zhang et al. (2024) studied the optimal mixing ratio of concrete mixed with coal gangue and fly ash and used SEM, AE, IRT, and other technologies to study its failure mechanism. Liu et al. (2024) conducted triaxial compression tests on the addition of coal gangue and fly ash backfilled at different temperatures and found that the cohesion of the cemented material showed a trend of first decreasing and then increasing with the increase in temperature. Li et al. (2023d) studied the properties of coal gangue and fly ash backfillers induced by microorganisms and determined the effects of different factors such as microbial concentration, curing time, and melting temperature on the compressive strength of backfillers.

Based on the above research background, this paper adopts a four-factor and four-level orthogonal test to study the cube compressive strength and splitting tensile strength of concrete mixed with coal gangue ceramic particles, coal gangue ceramic sand (CGS), steel fiber (SF), and fly ash and uses a range analysis, variance analysis, matrix analysis, and regression analysis to explore the optimal combination, strength of influence, and strength prediction model under different factor levels. In addition, the SEM technology is used to analyze the modification effect and strengthening mechanism of different materials on concrete to promote the wide application of solid waste such as coal gangue and fly ash in concrete.

2 Materials and methods

2.1 Materials

The cement used in the test was P.O.42.5 ordinary Portland cement; the initial setting time was 181 min; the final setting time was 266 min; and the volume stability was qualified. The selected coarse aggregate was ordinary gravel, particle size was 5–20 mm, fine aggregate selected was natural river sand, fineness modulus was 2.6, water is ordinary tap water; end hook steel fiber (SF) is selected, the length is 35 mm, the length–diameter ratio is 47, the tensile strength is 1,000–1800 MPa, and the production place is Hengshui, Hebei, China. The shape is shown in Figure 1A; coal gangue comes from Fuxin, Liaoning, China, and is used after crushing and screening. It is divided into ceramic sand (CGS) and ceramic particles (CG) according to different particle sizes. The particle size of CGS ranges from 0.5 to 4.5 mm, and that of CG ranges from 5 to 16 mm. The shapes of CG and CGS are shown in Figures 1B, C, respectively. According to ASTM C618, the fly ash is Class C fly ash (FA) and the production place is Zhengzhou, Henan, China, and its shape is shown in Figure 1D. The chemical composition of FA and cement is shown in Table 1.

2.2 Orthogonal test design and mix proportion

Numerous factors affect the performance of steel fiber concrete and composite solid waste, and comprehensive testing will result in a significant increase in the number of tests, whereas orthogonal testing uses a small number of tests to obtain the overall test information and a comprehensive conclusion and can obtain and verify the optimal results of the entire test range through various data analysis methods and calculations. The four factors are, therefore, CG and other qualities to replace coarse aggregate (Factor A), CGS and other qualities to replace fine aggregate (Factor B), steel fiber content (Factor C), and FA and other qualities to replace cement (Factor D). As a result, this paper uses a four-factor and four-level orthogonal test. According to the research results in the literature (Thi et al., 2021; Qiu J. et al., 2023; Li et al., 2023b; Li et al., 2023c), different levels are selected, and the specific orthogonal test table is shown in Table 2. The C30 concrete was designed according to JG/T 472-2015 (JG/T472-2015, 2015) and JGJ 55-2011 (JGJ 55-2011, 2011), as shown in Table 3.

2.3 Specimen preparation

The concrete was mixed by GB/T50080-2002 (GB/T50080-2002, 2007) by using a forced single horizontal shaft concrete mixer. Grease oil was used to lubricate the mold, the material was weighed Table 3 to determine the amount needed; coarse and fine aggregates; CG, CGS, and FA were added to mix; and finally SF was distributed uniformly. When everything is well-combined, water is added and stirred for an additional 3 minutes. Finally, the mold is filled with the mixture and shaken. The mold was taken out and placed in the regular curing room for preservation after 24 h of rest. Figure 2

10.3389/fmats.2024.1431648

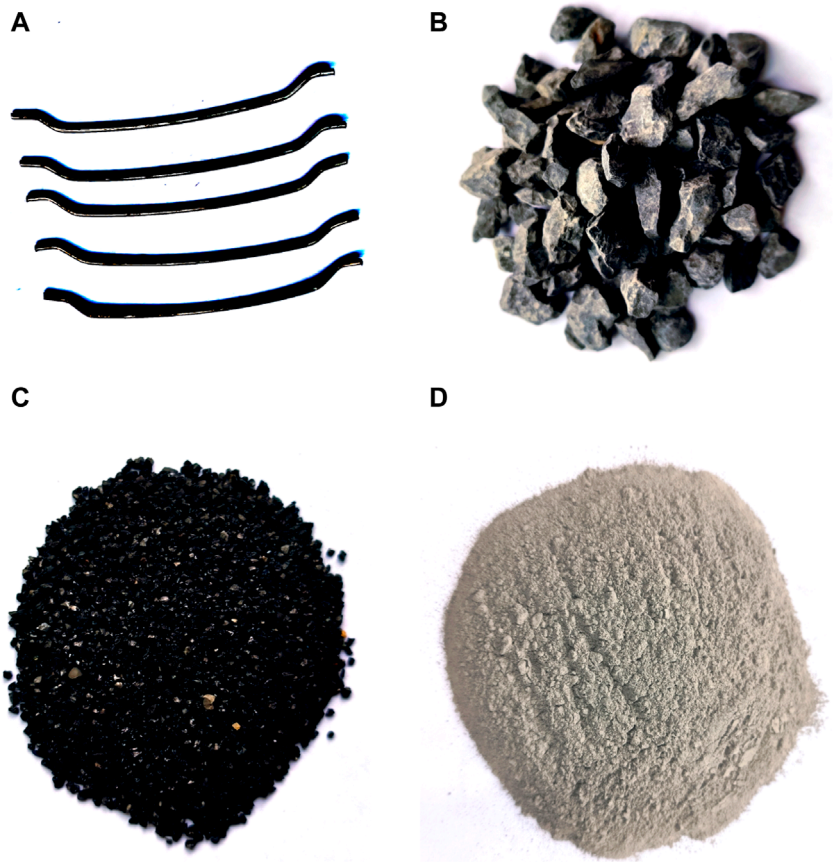

FIGURE 1
Raw materials **(A)** SF **(B)**. CG. **(C)** CGS. **(D)** FA.

TABLE 1 Chemical composition of FA and cement.

Material	CaO	SiO_2	Al_2O_3	Fe_2O_3	MgO	SO_3	Na_2O	Loss
Cement	59.44	22.06	6.19	3.61	1.26	1.02	0.26	1.75
FA	3.19	52.17	30.49	4.69	1.13	0.77	0.58	2.12

TABLE 2 Orthogonal test condition.

Level	Factor			
	A (%)	B (%)	C (%)	D (%)
1	15	10	0.30	10
2	20	15	0.60	15
3	25	20	0.90	20
4	30	25	1.20	25

depicts the procedure of creating a specimen. The mechanical properties were tested after 28 days of curing.

2.4 Experimental methods and main test instruments

2.4.1 Mechanical properties test

The cube compressive strength and splitting tensile strength are the two primary mechanical parameters tested, and the dimensions of the specimens are 100 mm by 100 mm by 100 mm. Each test group produces six specimens, three of which are utilized in the splitting tensile strength test and three for the cube compressive strength test. In total, 96 specimens were made.

According to GB/T 50,081-2019 (GB/T50081-2016, 2016), since the test specimen is non-standard, it is necessary to multiply the size conversion coefficient by 0.95 and 0.85, respectively. The loading equipment adopts a 2000-kN pressure testing machine, the loading speed of the compressive strength test is 0.5 MPa/s, the loading speed of splitting tensile strength is 0.05 MPa/s, and

10.3389/fmats.2024.1431648

TABLE 3 Mix ratio (kg/m^3).

Group	Water	Cement	FA	Stone	CG	Sand	CGS	SF
1	220	330	34.3	971.04	177.14	603.84	70.66	23.4
2	220	311.67	51.45	971.04	177.14	570.29	105.99	46.8
3	220	293.34	68.6	971.04	177.14	536.84	141.32	70.2
4	220	275	85.75	971.04	177.14	503.2	176.65	93.6
5	220	293.34	68.6	913.92	236.19	603.84	70.66	46.8
6	220	275	85.75	913.92	236.19	570.29	105.99	23.4
7	220	330	34.3	913.92	236.19	536.84	141.32	93.6
8	220	311.67	51.45	913.92	236.19	503.2	176.65	70.2
9	220	275	85.75	856.8	295.23	603.84	70.66	70.2
10	220	293.34	68.6	856.8	295.23	570.29	105.99	93.6
11	220	311.67	51.45	856.8	295.23	536.84	141.32	23.4
12	220	330	34.3	856.8	295.23	503.2	176.65	46.8
13	220	311.67	51.45	799.68	354.28	603.84	70.66	93.6
14	220	330	34.3	799.68	354.28	570.29	105.99	70.2
15	220	275	85.75	799.68	354.28	536.84	141.32	46.8
16	220	293.34	68.6	799.68	354.28	503.2	176.65	23.4

the maximum load is accurate to 0.01 MPa. The loading process is shown in Figure 3.

2.4.2 Microscopic test

SEM investigations were done by employing a Hitachi S-3400 scanning electron microscope. The acceleration voltage ranged from 0.3 to 30 kV, and in high vacuum (30-kV mode), the resolution was 3.0 nm. The resolution in the 3-kV high vacuum mode is 10 nm. Following the failure of the mechanical properties test, five small test blocks at various locations along the specimen's fracture surface were chosen as samples. These were then treated with gold spraying by using a plasma sputtering device and scanned using an S-3400 electron microscope. Figure 4 displays the sample and test apparatus.

3 Multivariate analysis of test results

The cured specimen was subjected to a loading test, and the results of the test are shown in Table 4. The range analysis method, variance analysis method, matrix analysis method, and regression analysis method are used to analyze the test results, discuss the primary and secondary degrees of influence of different factors on the mechanical properties of concrete, and obtain the optimal relationship under different combinations of factors.

3.1 Range analysis

The influence of the addition of CG, CGS, SF, and FA on the compressive strength and splitting tensile strength of concrete is studied and the test results are given in Table 4. The range analysis is calculated according to Equations 1, 2, and the calculation results are shown in Table 5.

$$Y_i = \frac{y_i}{N}, \tag{1}$$

$$R = \max[Y_i] - \min[Y_i], \tag{2}$$

where y_i is the sum of the results at the i level. Y_i is the mean of the sum of results at the i level. N is the group number. R is the range.

As can be seen from Table 5, the order of influence on the compressive strength of the cube is D > A > C > B. FA has the greatest influence on the compressive strength, SF has the least influence on the compressive strength, and the optimal combination is A4B2C4D1. The sequence of influences on the splitting tensile strength was C > B > D > A. SF had the greatest influence on the splitting tensile strength, while CG had the least influence. The optimal combination was A4B4C4D1. To more intuitively reflect the influence trend of different factors on the strength, the influence trend chart shown in Figure 5 is drawn according to the analysis results listed in Table 5.

FIGURE 2
Specimen making process.

When the CG substitution rate is 30% and the CGS substitution rate is 15%, the compressive strength is the highest. The splitting tensile strength is the highest when the CG substitution rate is 30% and the CGS substitution rate is 25%. The main reasons are as follows: the 24-h water absorption rate of coal gangue is 6.35%, which absorbs a large amount of water in the stirring process, thus forming an internal curing effect during curing (Li et al., 2021) and enhancing strength. The promoting effect is recorded as P1. The active substances such as Al2O3 and SiO2 inside the coal gangue react with the cement to produce the "volcanic ash" effect (Li et al., 2013; Yang et al., 2013), which improves the interfacial bond strength between the aggregate and the cement. The promotion effect is recorded as P2. Although the physical and chemical properties of coal gangue and natural aggregate are the same, there are a large number of acicular and flake particles in the coal gangue. With the increase in the replacement rate of natural aggregates by coal gangue, the content of acicular and flake particles in concrete increases and the specific surface area of aggregate increases, requiring more cement slurry to be coated. The increase in coal gangue plays a dispersive effect on the cementing material, which is not conducive to the development of the mechanical properties of the cementing material. The disadvantages of coal gangue as a concrete aggregate also appear, and this weakening effect is recorded as H1. From the fracture surface of concrete, it is found that a large number of cutting surfaces of coal gangue aggregates are displayed on the fracture development surface, as shown in Figure 6A, indicating that the self-stiffness of coal gangue is lower than that of natural aggregates. With the increase in the substitution rate, the strength of concrete decreases, and this weakening effect is recorded as H2. When P1 + P2 > H1 + H2, the concrete as a whole shows a promoting effect, that is, the strength increases. When P1 + P2 < H1 + H2, the weakening effect of concrete is obvious, that is, the strength decreases. Therefore, to ensure the strength grade of concrete, it is necessary to control the amount of coal gangue in concrete reasonably.

When SF content is 1.2%, the compressive strength and splitting tensile strength are the highest. The main reasons are as follows: the addition of steel fiber changes the form of compressive failure of concrete, the concrete cracks but does not disperse after failure, and the compressive toughness is significantly improved, as shown in Figure 6B. The analysis of the crack development process of the steel fiber shows that when the steel fiber is parallel to the interface crack, it cannot strengthen the crack resistance. When the crack enters the hardened cement slurry, the steel fiber across the crack begins to strengthen the effect, slowing down the expansion rate of the crack, but the crack system in the specimen becomes unstable. With the gradual increase in deformation, the specimen reaches the maximum stress it can withstand, i.e., the ultimate strength of concrete. At this time, the cracks expand rapidly, the macrocracks increase, and the steel fibers across the cracks effectively prevent the development of cracks so that the toughness of the specimen is improved. As the macroscopic crack continues to increase, the steel fiber is gradually pulled out, as shown in Figure 6C. In summary, the strengthening effect of the steel fiber can only be played when the specimen is stressed to reach the ultimate strength and the crack extends to the cement stone, which is

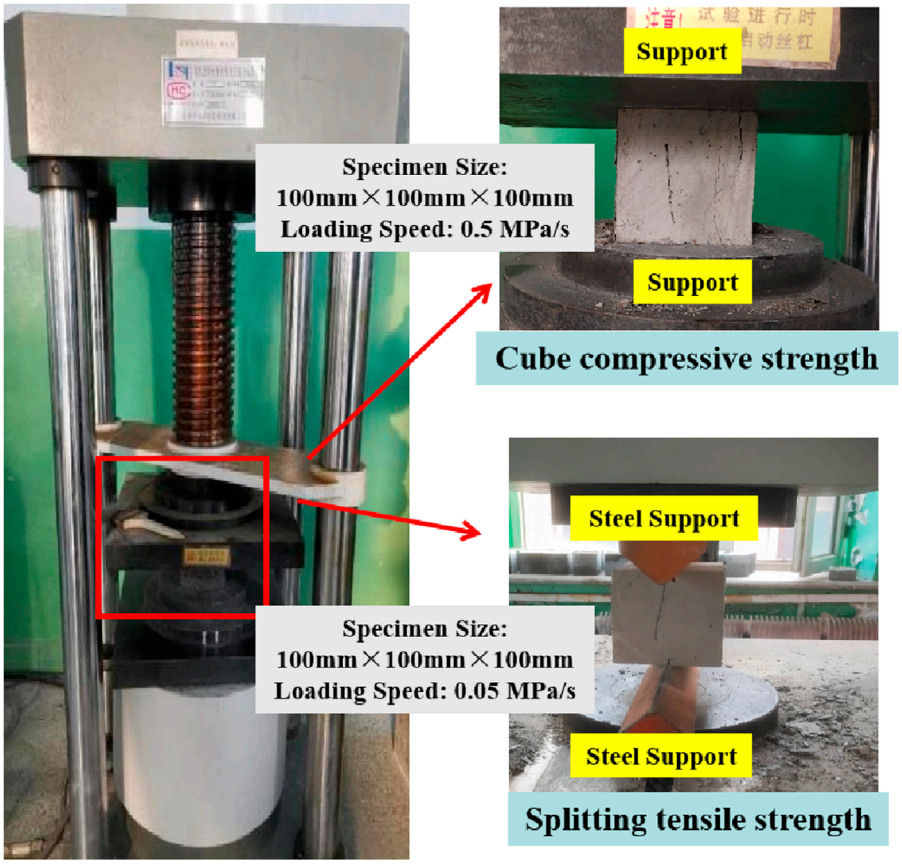

FIGURE 3
Mechanical property test.

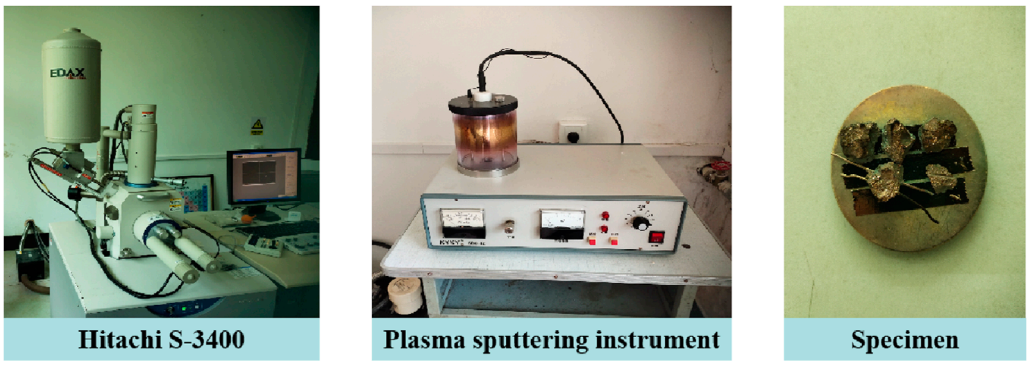

FIGURE 4
Test instruments and specimen.

also the reason why the compressive strength of the steel fiber is increased little and the tensile strength of the steel fiber is increased greatly.

When the FA content is 10%, the compressive strength and splitting tensile strength are the highest. The main reason is that the average particle size of FA is much smaller than that of coal gangue and natural aggregates, so FA can be evenly filled to form a close packing system between the aggregates so that the secondary hydration reaction is more adequate. However, with the increase in the substitution rate of FA, the same amount of cement cannot completely produce a volcanic ash effect with FA, resulting in a certain amount of pores and cracks between the particles in FA and the hydration products, which reduces the compactness of the mortar.

10.3389/fmats.2024.1431648

TABLE 4 Test results.

Group	Factor				Cube compressive strength/MPa	Splitting tensile strength/MPa
	A/%	B/%	C/%	D/%		
1	15	10	0.30	10	30.30	1.64
2	15	15	0.60	15	30.76	1.83
3	15	20	0.90	20	30.50	2.03
4	15	25	1.20	25	31.86	2.47
5	20	10	0.60	20	28.91	1.96
6	20	15	0.30	25	29.74	1.91
7	20	20	1.20	10	37.37	2.43
8	20	25	0.90	15	34.65	2.05
9	25	10	0.90	25	32.03	2.10
10	25	15	1.20	20	35.45	2.12
11	25	20	0.30	15	35.25	1.78
12	25	25	0.60	10	37.45	2.08
13	30	10	1.20	15	38.74	1.98
14	30	15	0.90	10	40.52	2.51
15	30	20	0.60	25	31.83	2.17
16	30	25	0.30	20	31.89	2.23

TABLE 5 Range analysis results.

Performance indicator	Factor	A	B	C	D
Cube compressive strength	Y_1	30.85	32.50	31.79	36.41
	Y_2	32.67	34.12	32.24	34.85
	Y_3	35.04	33.74	34.43	31.69
	Y_4	35.75	33.96	35.85	31.37
	R	4.89	1.62	4.06	5.04
	Influence order	D > A > C > B			
Splitting tensile strength	Y_1	1.99	1.92	1.89	2.17
	Y_2	2.09	2.09	2.01	1.91
	Y_3	2.02	2.10	2.17	2.09
	Y_4	2.22	2.21	2.25	2.16
	R	0.23	0.29	0.36	0.26
	Influence order	C > B > D > A			

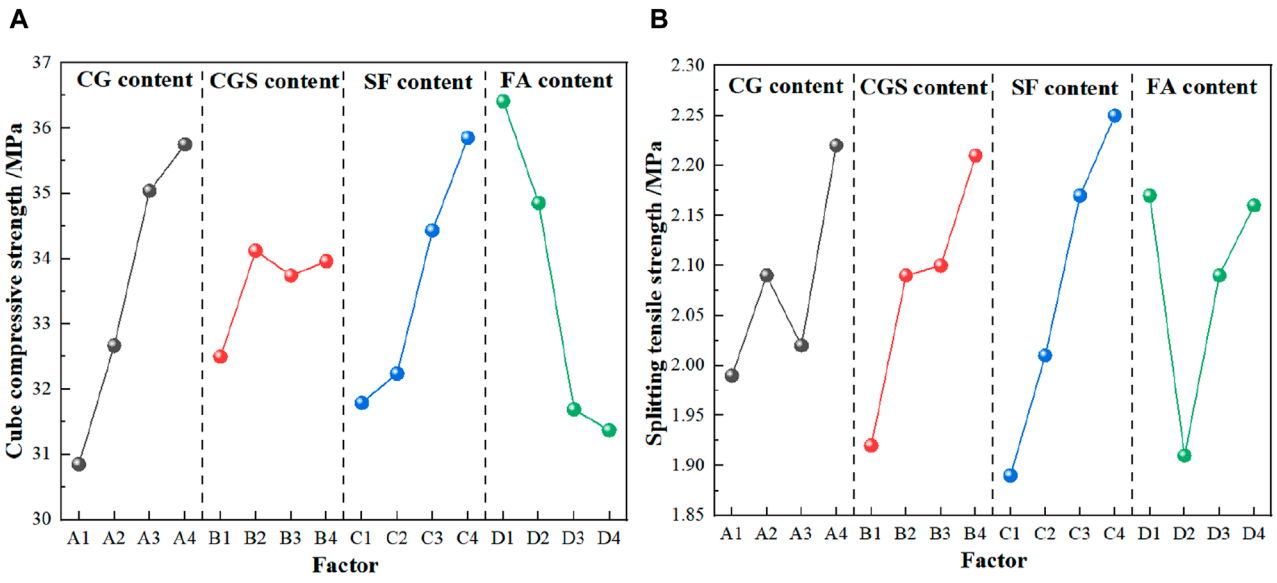

FIGURE 5
Influence trend. **(A)** Cube compressive strength. **(B)** Splitting tensile strength.

FIGURE 6
Failure mode of concrete. **(A)** Coal gangue burst. **(B)** Compressive strength test. **(C)** Steel fiber pulling.

3.2 Variance analysis

Range analysis can judge the influence of different factors on the intensity and the optimal combination, while variance analysis can accurately estimate the change in test results and the cause of error, which is a supplement to range analysis. According to the method described by Li et al. (2023b), the sum of squared deviations (SSDs), degree of freedom (Fd), and mean square (MS) are calculated. The significance level was selected according to the F value distribution table in optimal design and analysis of experiments (Ren, 2003), and the calculation results are shown in Table 6.

For the compressive strength, the influence order of all factors was FA > CG > SF > CGS, and the F value of FA and CG was greater than F0.05 (3.3), indicating that FA and CG had a major impact on the compressive strength. For the splitting tensile strength, the influence order of all factors was SF > CGS > FA > CG, and the F value of SF was close to F0.10 (3.3), indicating that SF had a minor impact on the splitting tensile strength. The conclusion of variance analysis and range analysis is the same, and the reliability of the analysis results is verified again.

3.3 Matrix analysis

The matrix analysis method does not use the measured data from the test and processes the range analysis results in the form of a matrix for analysis. According to the range analysis results in Table 5, a three-layer data structure model is established, which

10.3389/fmats.2024.1431648

TABLE 6 Variance analysis results.

Performance indicator	Factor	SSD	Fd	MS	F	Significance criterion	Significance level
Cube compressive strength	A	60.41	3	20.14	12.80	F0.05 (3.3) = 9.28 F0.10 (3.3) = 5.39	**
	B	6.54	3	2.18	1.39		—
	C	43.53	3	14.51	9.22		*
	D	72.39	3	24.13	15.33		**
	Error	4.72	3	1.57			
Splitting tensile strength	A	0.13	3	0.04	1.73	F0.05 (3.3) = 9.28 F0.10 (3.3) = 5.39	—
	B	0.20	3	0.07	2.67		—
	C	0.40	3	0.13	5.33		(*)
	D	0.16	3	0.05	2.13		—
	Error	0.08	3	0.03			

Note: ** represents a major impact, ** represents a moderate impact, (*) represents a minor impact, and — represents no impact.

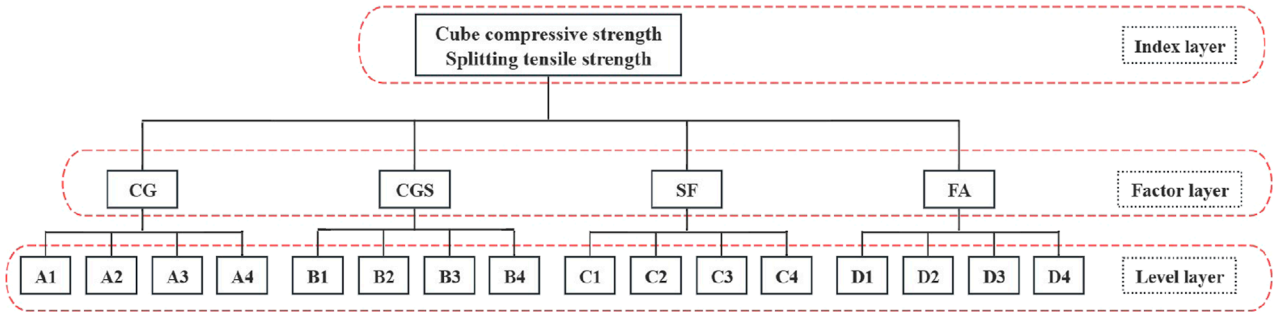

FIGURE 7
Data structure hierarchy.

includes an index layer, factor layer, and level layer, as shown in Figure 7. A three-layer matrix was established according to the levels of the data structure, and the influence weights of each factor level on the test indicators were obtained by multiplying with MATLAB, as shown in Table 7. By comparing the weight values, the influence degree of each factor level on the test indicators and the optimal combination were obtained.

The weight of each factor is summed to obtain the weight of the factor. As can be seen from Table 7, the order of each factor of compressive strength from the largest to the smallest is D > A > C > B, that is, FA > CG > SF > CGS. By comparing the weight of each level, it can be observed that the optimal combination is A4B2C4D1, that is, the CG substitution rate is 30%, CGS substitution rate is 15%, SF content is 1.2%, and FA substitution rate is 10%. The order of splitting tensile strength factors from large to small is C > B > D > A, that is, SF > CGS > FA > CG. The optimal combination is A4B4C4D1, that is, the CG substitution rate is 30%, CGS substitution rate is 25%, SF content is 1.2%, and FA substitution rate is 10%. The conclusion is consistent with range and variance analyses.

3.4 Regression analysis

In this paper, IBM SPSS statistics is used to analyze the mechanical properties by multiple linear regression.

Suppose the linear regression result can be written as Equation 3

$$\begin{bmatrix} y_1 \\ y_2 \\ y_3 \\ y_4 \\ y_5 \end{bmatrix} = \begin{bmatrix} 1 & x_{11} & x_{12} & x_{13} & x_{14} \\ 1 & x_{21} & x_{22} & x_{23} & x_{24} \\ 1 & x_{31} & x_{32} & x_{33} & x_{34} \\ 1 & x_{41} & x_{42} & x_{43} & x_{44} \\ 1 & x_{51} & x_{52} & x_{53} & x_{54} \end{bmatrix} \cdot \begin{bmatrix} \alpha_0 \\ \alpha_1 \\ \alpha_2 \\ \alpha_3 \\ \alpha_4 \end{bmatrix}. \quad (3)$$

By establishing the corresponding eigenmatrix, the equation is simplified to

$$y = \alpha_0 + \alpha_1 x_1 + \alpha_2 x_2 + \alpha_3 x_3 + \alpha_4 x_4, \quad (4)$$

where y is the mechanical property; α_0, α_1, α_2, α_3, and α_4 are the regression coefficients; x_1, x_2, x_3, and x_4 are CG, CGS, SF, and FA, respectively.

TABLE 7 Matrix analysis results.

Factor	Cube compressive strength		Splitting tensile strength	
	Weighted value	Total	Weighted value	Total
A1	0.0720	0.3133	0.0482	0.2015
A2	0.0762		0.0506	
A3	0.0817		0.0489	
A4	0.0834		0.0538	
B1	0.0251	0.1038	0.0586	0.2546
B2	0.0264		0.0638	
B3	0.0261		0.0647	
B4	0.0262		0.0675	
C1	0.0616	0.2601	0.0716	0.3154
C2	0.0624		0.0762	
C3	0.0667		0.0823	
C4	0.0694		0.0853	
D1	0.0875	0.3229	0.0667	0.2539
D2	0.0838		0.0586	
D3	0.0762		0.0632	
D4	0.0754		0.0654	

The experimental values of compressive strength and splitting tensile strength are substituted into Equation 4, and the correlation regression coefficient is obtained. The regression equation of compressive strength is shown in Equation 5, and the regression equation of splitting tensile strength is shown in Equation 6.

$$y = 27.302 + 34.112x_1 + 8.058x_2 + 479.042x_3 - 36.582x_4, \quad (5)$$

$$y = 1.126 + 1.245x_1 + 1.745x_2 + 41.417x_3 + 0.335x_4. \quad (6)$$

The compressive strength and splitting tensile strength were predicted by regression equation and the values compared with the test values. The accuracy of the model was determined by the residual test. The comparison results are shown in Table 8, and the graph shown in Figure 8 was drawn for a more intuitive analysis.

As can be seen from Table 8; Figure 8, the error of the compressive strength equation and the variance of the splitting tensile strength are 2.58% and 5.53%, respectively. It can also be seen from Figure 8B that there is a large deviation between the results of some experimental groups and the predicted results.

The main reasons for the error are as follows: ① uneven dispersion of the material. The steel fiber is easy to cluster, resulting in uneven dispersion; when coal gangue is coated with coal gangue powder, it will absorb water and affect the efficiency of the hydration reaction. ② Accidental error in the test process: During the test, loading speed, data measurement, calculation accuracy, and other reasons may also cause errors in the test results.

But the overall error is still within 6%, that is, the accuracy of the equation is high. In conclusion, both regression models can predict concrete strength well within the range of factors selected in this paper.

4 Microstructure analysis

The macroscopic mechanical strength of concrete is determined by the properties of the concrete matrix and interfacial transition zone (ITZ). The changes in the ITZ after the addition of CG, CGS, SF, and FA are analyzed from the microscopic level, and the strengthening mechanism of different materials on concrete strength is further discussed, which provides a theoretical basis for the application of solid waste and steel fiber in concrete.

4.1 Micro-morphology of different materials

4.1.1 Coal gangue

The rigidity of coal gangue is lower than that of the natural aggregates (Di et al., 2016), and fractures occur on their own under the action of external loads. Figure 9 shows the microscopic morphology of the coal gangue fracture surface magnified by 15 times and 90 times, respectively. It can be seen from Figure 9 that obvious cracks appear on the fracture surface of the coal gangue, indicating that fine particles are attached. Therefore, when the replacement rate of coal gangue is too high, the promotion effect brought by internal curing and volcanic ash is far less than the weakening effect of its stiffness, that is, the macro mechanical property strength decreases.

4.1.2 Fly ash

The particle size of fly ash is small, and it can be well-dispersed into the concrete to fill the pores and micro-cracks. As can be seen from Figure 10, fly ash uniformly disperses into the matrix, reacts with the cement slurry, and generates C-S-H gel and needle-like AFt through the pozzolanic effect. These materials are connected, thus enhancing the stability of the mortar structure.

4.1.3 Steel fiber

The steel fiber incorporated into concrete needs to be coated with cement slurry, which is also confirmed by the cement slurry attached to the surface of the steel fiber, as shown in Figure 11. The steel fibers bear the external load through the bonding force generated by the cement paste and the hoop effect generated by the lap between the steel fibers. When the cracks enter the hardened cement paste, the steel fibers across the cracks begin to play a strengthening role and

TABLE 8 Comparison of test values and predicted values.

Group	Cube compressive strength				Splitting tensile strength			
	Experimental value (MPa)	Predicted value (MPa)	Residual error (MPa)	Relative square (%)	Experimental value (MPa)	Predicted value (MPa)	Residual error (MPa)	Relative square (%)
1	30.30	31.00	0.70	2.33	1.64	1.65	0.00	0.13
2	30.76	31.01	0.26	0.84	1.83	1.87	0.04	2.21
3	30.50	31.03	0.52	1.72	2.03	2.10	0.07	3.34
4	31.86	31.04	−0.83	2.59	2.47	2.33	−0.14	5.78
5	28.91	30.49	1.58	5.45	1.96	1.87	−0.10	4.88
6	29.74	27.62	−2.11	7.10	1.91	1.84	−0.06	3.27
7	37.37	37.83	0.46	1.22	2.43	2.25	−0.18	7.37
8	34.65	34.96	0.31	0.90	2.05	2.23	0.18	8.75
9	32.03	31.80	−0.23	0.73	2.10	2.07	−0.03	1.32
10	35.45	35.47	0.03	0.07	2.12	2.26	0.14	6.52
11	35.25	33.39	−1.85	5.26	1.78	1.96	0.18	10.03
12	37.45	37.06	−0.39	1.04	2.08	2.16	0.07	3.50
13	38.74	38.60	−0.14	0.35	1.98	2.22	0.25	12.43
14	40.52	39.40	−1.13	2.78	2.51	2.17	−0.34	13.66
15	31.83	32.88	1.04	3.27	2.17	2.18	0.02	0.72
16	31.89	33.67	1.78	5.57	2.23	2.13	−0.10	4.62
Mean relative square (%)	2.58				5.53			

10.3389/fmats.2024.1431648

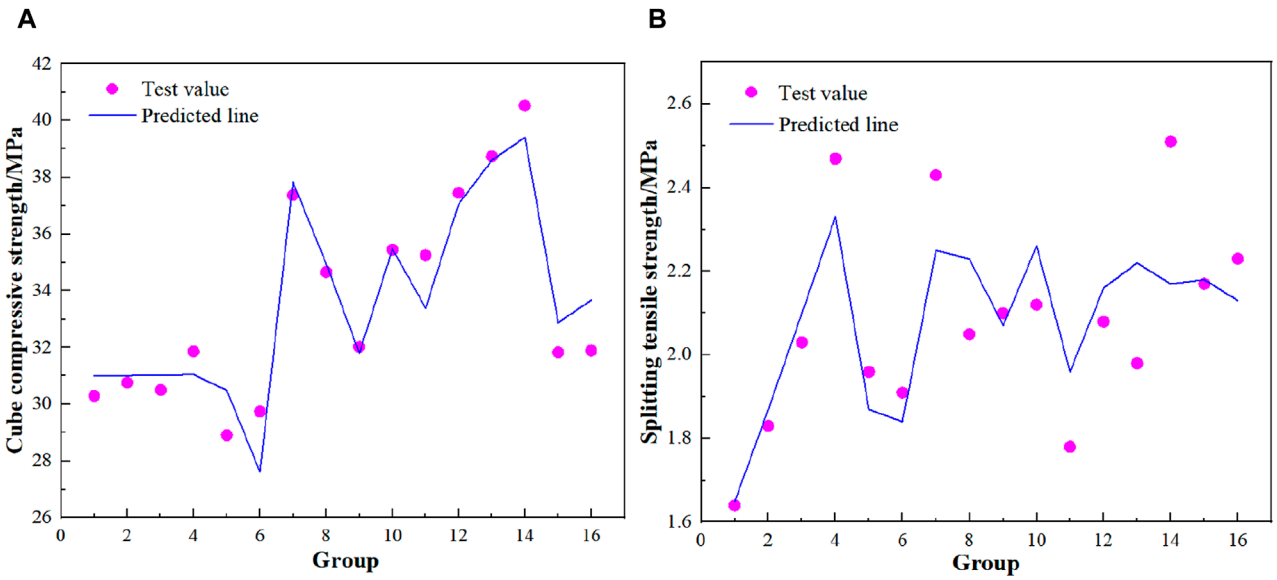

FIGURE 8
Comparison of test values and predicted values. **(A)** Cube compressive strength. **(B)** Splitting tensile strength.

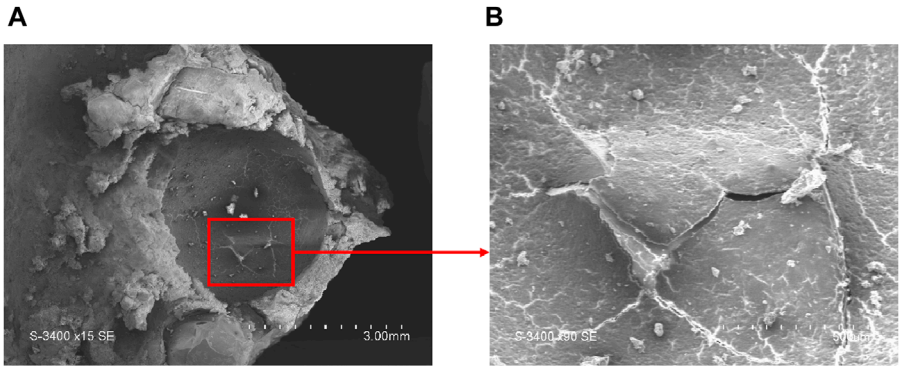

FIGURE 9
Micro-morphology of coal gangue. **(A)** 15 times. **(B)** 90 times.

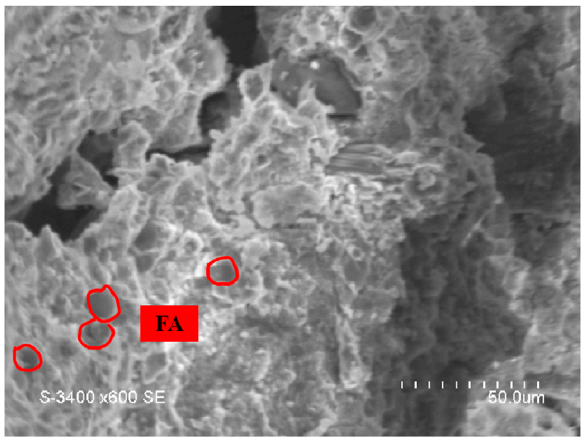

FIGURE 10
Micro-morphology of fly ash.

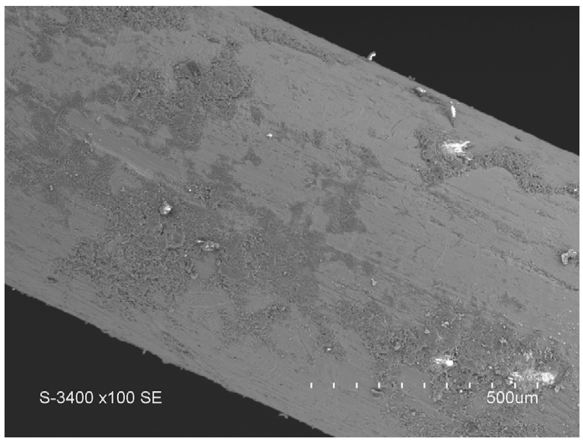

FIGURE 11
Micro-morphology of steel fiber.

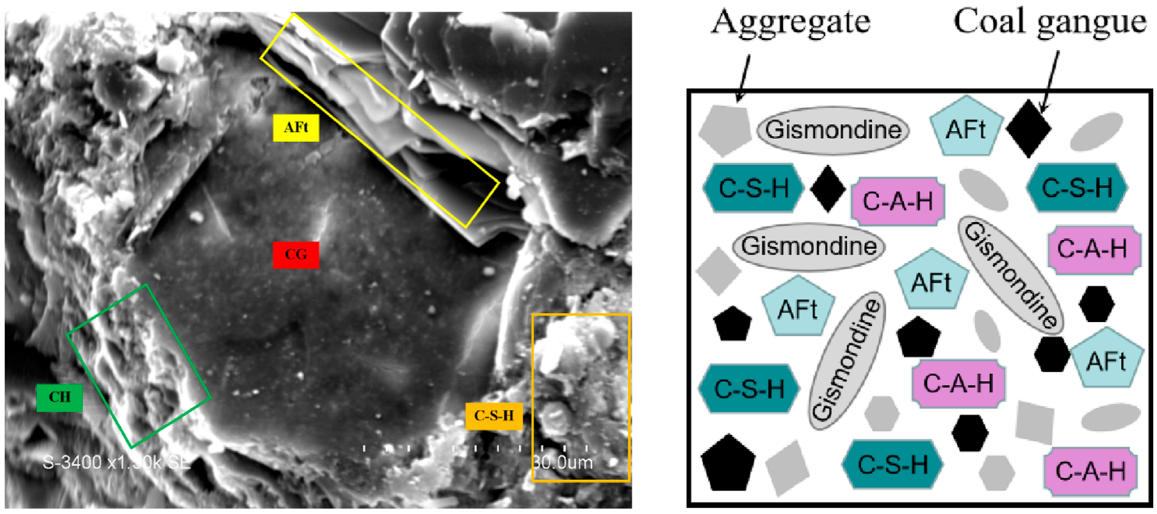

FIGURE 12
Influence mechanism of CG on ITZ. **(A)** Influence mechanism of coal gangue. **(B)** Influence mechanism model (Li et al., 2023d).

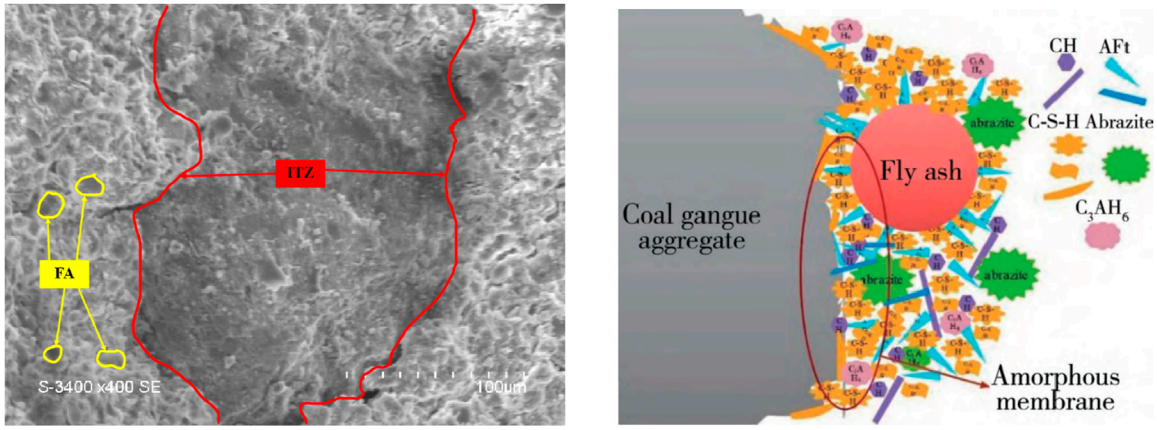

FIGURE 13
Influence mechanism of FA on ITZ. **(A)** Influence mechanism of fly ash. **(B)** Influence mechanism model (Li et al., 2023d).

absorb a lot of energy, which is reflected in the macro improvement of concrete strength.

4.2 Influence mechanism of different materials on ITZ

4.2.1 Coal gangue

The strengthening effect of coal gangue and fly ash as solid waste is mainly due to the hydration reaction of cement and the pozzolanic effect of solid waste. The hydration reaction of cement consumes tricalcium silicate (C3S), terrarium-aluminum ferrite (C_4AF), and other substances to produce AFt, C-S-H, and C-A-H, as shown in Figure 12A while the volcanic ash effect of coal gangue consumes SiO_2, Al_2O_3, and other active substances to produce gismondine, as shown in Figure 12B. These substances interweave with each other so that the density of the matrix is increased and the strength is increased macroscopically.

4.2.2 Fly ash

Fly ash particles are distributed among cement particles. In the alkaline environment of $Ca(OH)_2$ generated after cement hydration, the active substances SiO_2 and Al_2O_3 in fly ash undergo a secondary hydration reaction, which consumes $Ca(OH)_2$ in the specimen, inhibits the growth of $Ca(OH)_2$ grains, and reduces ITZ thickness, as shown in Figure 13A. With the continuous consumption of $Ca(OH)_2$, the amount of the gel substance generated increases. The fly ash scattered near the ITZ plays the role of a crystal nucleus and becomes the skeleton, which is combined with the amorphous film, and the gel gradually compacts to form an amorphous membrane and adheres to the surface of the aggregate, as shown in Figure 13B is Qiu et al. (2023b), of the model.

4.2.3 Steel fiber

Influence mechanism of coal gangue on ITZ as shown in Figure 12. Influence mechanism of fly ash on ITZ as shown in Figure 13. Influence mechanism of steel fiber on ITZ as shown

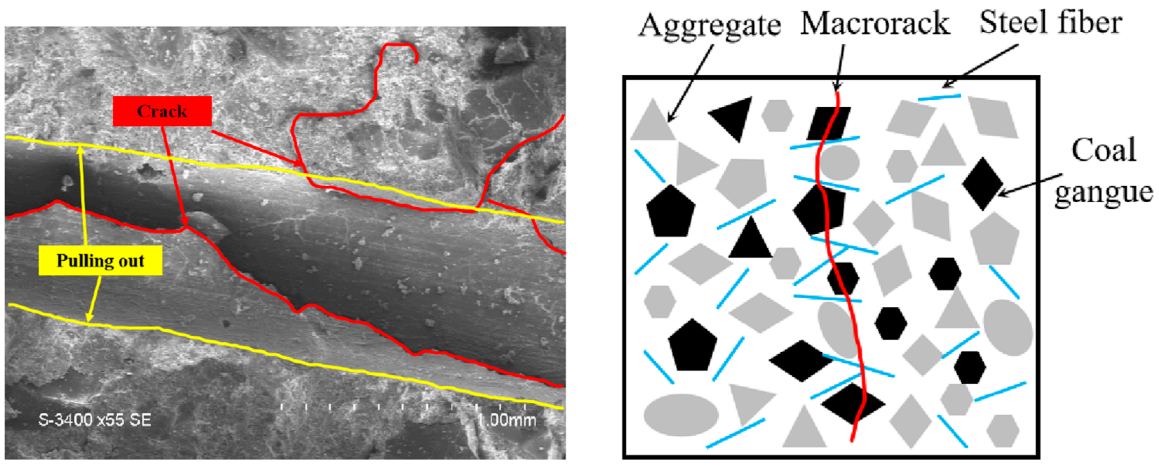

FIGURE 14
Influence mechanism of SF on ITZ. **(A)** Influence mechanism of steel fiber. **(B)** Influence mechanism model (Li et al., 2023d).

in Figure 14. The steel fibers randomly distributed in the concrete matrix overlap with each other to form a hoop effect, which can inhibit the formation, expansion, and extension of cracks. As shown in Figure 14A, the steel fibers are pulled out, the concrete has obvious pull-out marks, and there are a large number of cracks around the pull-out track and pull-out path, which can be observed. When the crack extends around the steel fiber, more energy is needed to pull out or break the steel fiber, that is, the steel fiber across the crack inhibits the expansion of the crack. The influence mechanism model of the steel fiber on the late through the crack is shown in Figure 14B.

5 Conclusion

To study the modification effect and microscopic mechanism of composite solid waste and steel fiber on the mechanical properties of concrete, the orthogonal test was used to conduct experimental research on the dosage of different materials such as CG, CGS, SF, and FA and analyze the microstructure and strengthening mechanism of different materials. According to the test results, the conclusions are as follows:

(1) The influence degree of different factors on mechanical properties was obtained through range analysis, variance analysis, and matrix analysis. The results show that the optimal combination of the CG substitution rate is 30%, the CGS substitution rate is 15%, SF content is 1.2%, and FA substitution rate is 10% for cube compressive strength. For the splitting tensile strength, the optimal combination is a CG substitution rate of 30%, CGS substitution rate of 25%, SF content of 1.2%, and FA substitution rate of 10%.

(2) The regression equations were obtained through regression analysis, and the errors were 2.58% and 5.53% according to the residual test analysis. The strength of composite solid waste and steel fiber-reinforced concrete can be predicted within the horizontal range selected by the orthogonal test.

(3) Solid waste coal gangue and fly ash improve the strength of concrete through the hydration reaction of Portland cement and the volcanic ash effect, and the generated active substances are interwoven and attached to the aggregate surface, which improves the strength of concrete on a macro level.

(4) The randomly distributed steel fibers overlap with each other, forming a hoop effect to transfer stress in the matrix, requiring more energy to break or pull out the steel fibers across the cracks, thus restraining the expansion of cracks and improving the strength of concrete on a macro level.

Data availability statement

The original contributions presented in the study are included in the article/Supplementary Material; further inquiries can be directed to the corresponding author.

Author contributions

QZ: writing–review and editing, funding acquisition, formal analysis, and conceptualization. LC: writing–review and editing, writing–original draft, investigation, formal analysis, and data curation. XW: writing–review and editing, methodology, and investigation. SZ: writing–review and editing and investigation. FL: writing–review and editing and investigation.

Funding

The author(s) declare that financial support was received for the research, authorship, and/or publication of this article. This project is financially supported by the Science and Technology Development Plan of Jilin Province (YDZJ202302CXJD052).

Conflict of interest

Author XW was employed by Shanxi Architectural Design and Research Institute Co., Ltd.

The remaining authors declare that the research was conducted in the absence of any commercial or financial relationships that could be construed as a potential conflict of interest.

Publisher's note

References

Di, W., Zhang, Y., and Liu, Y. (2016). Mechanical performance and ultrasonic properties of cemented gangue backfill with admixture of fly ash. *Ultrasonics* 64, 89–96. doi:10.1016/j.ultras.2015.08.004

GB/T50080-2002 (2007). *Standard for performance test method of ordinary concrete mixture*. Beijing, China: China Academy of Building Research. (in Chinese).

GB/T50081-2016 (2016). "Test method standard for mechanical properties of ordinary concrete,". Beijing: Beijing China Architecture and Construction Press. (in Chinese).

Golewski, G. L. (2022). The role of pozzolanic activity of siliceous fly ash in the formation of the structure of sustainable cementitious composites. *Sustain. Chem.* 3 (4), 520–534. doi:10.3390/suschem3040032

Golewski, G. L. (2023a). Study of strength and microstructure of a new sustainable concrete incorporating pozzolanic materials. Structural Engineering and Mechanics. *Int'l J.* 86 (4), 431–441. doi:10.12989/sem.2023.86.4.431

Golewski, G. L. (2023b). Examination of water absorption of low volume fly ash concrete (LVFAC) under water immersion conditions. *Mater. Res. Express* 10 (8), 085505. doi:10.1088/2053-1591/acedef

Golewski, G. L. (2023c). Assessing of water absorption on concrete composites containing fly ash up to 30% in regards to structures completely immersed in water. *Case Stud. Constr. Mater.* 19, e02337. doi:10.1016/j.cscm.2023.e02337

Golewski, G. L. (2023d). The effect of the addition of coal fly ash (CFA) on the control of water movement within the structure of the concrete. *Materials* 16 (15), 5218. doi:10.3390/ma16155218

Golewski, G. L. (2024). Enhancement fracture behavior of sustainable cementitious composites using synergy between fly ash (FA) and nanosilica (NS) in the assessment based on digital image processing procedure. *Theor. Appl. Fract. Mech.* 131, 104442. doi:10.1016/j.tafmec.2024.104442

Guo, L., Zhou, M., Wang, X., and Jia, H. (2022). Preparation of coal gangue-slag-fly ash geopolymer grouting materials. *Constr. Build. Mater.* 328, 126997. doi:10.1016/j.conbuildmat.2022.126997

JGJ 55-2011 (2011). *Common concrete mix design code*. Beijing: China Building and Construction Press. (in Chinese).

JG/T472-2015 (2015). *Steel fiber reinforced concrete*. Beijing: Standards Press of China. (in Chinese).

Li, J., Chen, L., Luo, J., Zhu, W., Fan, X., Zhu, Y., et al. (2023d). Mechanical properties and microscopic characteristics of steel fiber coal gangue concrete. *Front. Mater.* 10, 1211129. doi:10.3389/fmats.2023.1211129

Li, J., Chen, L., Luo, J., Zhu, Y., Fan, X., and Hu, G. (2023c). Study on mechanical properties and microstructure of steelpolypropylene fiber coal gangue concrete. *Front. Mater.* 10, 1281372. doi:10.3389/fmats.2023.1281372

Li, J., Chen, L., Wang, X., Hu, G., Wang, Z., Guo, J., et al. (2023b). Effect of compounding conductive materials on the mechanical properties of concrete and the microscopic mechanism. *Constr. Build. Mater.* 377, 131000. doi:10.1016/j.conbuildmat.2023.131000

Li, J., Luo, J., Chen, L., Fan, X., Zhu, Y., and Wang, X. (2024). Axial-compression performance and numerical-simulation analysis of steel tube coal gangue concrete column. *J. Constr. Steel Res.* 216, 108612. doi:10.1016/j.jcsr.2024.108612

Li, J., Zhao, E., Niu, J., and Wan, C. (2021). Study on mixture design method and mechanical properties of steel fiber reinforced self-compacting lightweight aggregate concrete. *Constr. Build. Mater.* 267, 121019. doi:10.1016/j.conbuildmat.2020.121019

Li, M., Peng, Y., Zhang, J., Zhao, Y., Wang, Z., Guo, Q., et al. (2023a). Properties of a backfill material prepared by cementing coal gangue and fly ash through microbial-induced calcite precipitation. *Constr. Build. Mater.* 384, 131329. doi:10.1016/j.conbuildmat.2023.131329

Li, Y., Yao, Y., Liu, X., Sun, H., and Ni, W. (2013). Improvement on pozzolanic reactivity of coal gangue by integrated thermal and chemical activation. *Fuel* 109 (jul), 527–533. doi:10.1016/j.fuel.2013.03.010

Liu, W., Hu, Z., Liu, C., Huang, X., and Hou, J. (2024). Mechanical properties under triaxial compression of coal gangue-fly ash cemented backfill after cured at different temperatures. *Constr. Build. Mater.* 411, 134268. doi:10.1016/j.conbuildmat.2023.134268

Moussadik, A., El Fadili, H., Saadi, M., and Diouri, A. (2024). Lightweight aerated concrete based on activated powders of coal gangue and fly ash. *Constr. Build. Mater.* 417, 135333. doi:10.1016/j.conbuildmat.2024.135333

Nayanathara Thathsarani Pilapitiya, P. G. C., and Ratnayake, A. S. (2024). The world of plastic waste: a review. *Clean. Mater.* 11, 100220. doi:10.1016/j.clema.2024.100220

Patel, K. S., Shah, D. B., Joshi, S. J., et al. (2023). Developments in 3D printing of carbon fiber reinforced polymer containing recycled plastic waste: a review. *Clean. Mater.* 9, 100207. doi:10.1016/j.clema.2023.100207

Qiu, J., Huo, Y., Feng, Z., Li, L., Wang, J., Zhang, Y., et al. (2023a). Study on the modification effect and mechanism of a compound mineral additive and basalt fiber on coal gangue concrete. *Buildings* 13 (11), 2756. doi:10.3390/buildings13112756

Qiu, J., Zhu, M., Zhou, Y., et al. (2023b). Modification effect of fly ash on interfacial transition zone of coal gangue concrete. *Mater. Rev.* 37 (02), 75–81. (in Chinese). doi:10.11896/cldb.21050280

Ren, L. (2003). *Experiment optimization design and analysis*. USA: Higher Education Press. (in Chinese).

Roy, A., and Islam, G. M. S. (2024). Geopolymer using different size fractions of recycled brick-based mixed demolition waste. *Clean. Mater.* 11, 100224. doi:10.1016/j.clema.2024.100224

Song, Q., Li, J., and Zeng, X. (2015). Minimizing the increasing solid waste through zero waste strategy. *J. Clean. Prod.* 104, 199–210. doi:10.1016/j.jclepro.2014.08.027

Thi, N. N., Truong, S. B., and Do Minh, N. (2021). Reusing coal ash of thermal power plant in a pavement base course. *J. King Saud University-Engineering Sci.* 33 (5), 346–354. doi:10.1016/j.jksues.2020.09.017

Wang, J., Ren, C., Huang, T., Li, X., Cao, W., Zhu, Y., et al. (2024). Performances of concrete with binder and/or aggregates replacement by all-solid waste materials. *J. Clean. Prod.* 450, 141929. doi:10.1016/j.jclepro.2024.141929

Yang, Q., Miaoxiong, L., and Luo, Y. (2013). Effects of surface-activated coal gangue aggregates on properties of cement-based materials. *J. Wuhan Univ. Technol.* 28 (006), 1118–1121. doi:10.1007/s11595-013-0830-2

Yu, L., Xia, J., Xia, Z., Chen, M., Wang, J., and Zhang, Y. (2022). Study on the mechanical behavior and micro-mechanism of concrete with coal gangue fine and coarse aggregate. *Constr. Build. Mater.* 338, 127626. doi:10.1016/j.conbuildmat.2022.127626

Zhang, L., Lai, X., Pan, J., Shan, P., Zhang, Y., Zhang, Y., et al. (2024). Experimental investigation on the mixture optimization and failure mechanism of cemented backfill with coal gangue and fly ash. *Powder Technol.* 440, 119751. doi:10.1016/j.powtec.2024.119751

Zhu, M., Qiu, J., and Chen, J. (2022). Effect and mechanism of coal gangue concrete modification by basalt fiber. *Constr. Build. Mater.* 328, 126601. doi:10.1016/j.conbuildmat.2022.126601